Optical and Quantum Electronics **24** *(1992) S245–S272*

AN INVITED PAPER

Controlling spontaneous emission and threshold-less laser oscillation with optical microcavities

H. YOKOYAMA, K. NISHI, T. ANAN, Y. NAMBU
Opto-Electronics Research Laboratories, NEC Corporation, 34 Miyukigaoka, Tsukuba 305, Japan

S. D. BRORSON*, E. P. IPPEN
Department of Electrical Engineering and Computer Science and Research Laboratory of Electronics, Massachusetts Institute of Technology, Cambridge, MA 02139, USA

M. SUZUKI†
Functional Devices Research Laboratories, NEC Corporation 4-1-1 Miyazaki, Miyamae-ku, Kawasaki 213, Japan

Received 24 June; revised and accepted 11 October 1991

We describe the alteration of spontaneous emission of materials in optical microcavities having dimensions on the order of the emitted wavelength. Particular attention is paid to one-dimensional optical confinement structures with pairs of planar reflectors (planar microcavities). The presence of the cavity causes great modifications in the emission spectrum and spatial emission intensity distribution accompanied by changes in the spontaneous emission lifetime. Experimental results are shown for planar microcavities containing GaAs quantum wells or organic dye-embedded Langmuir–Brodgett films as light emitting layers. Also discussed are the laser oscillation properties of microcavities. A remarkable increase in the spontaneous emission coupling into the laser oscillation mode is expected in microcavity lasers. A rate equation analysis shows that increasing the coupling of spontaneous emission into the cavity mode causes the disappearance of the lasing threshold in the input–output curve. Experimentally verification is presented using planar optical microcavities confining an organic dye solution. The coupling ratio of spontaneous emission into a laser mode increases to be as large as 0.2 for a cavity having a half wavelength distance between a pair of mirrors. At this point, the threshold becomes quite fuzzy. Differences between the spontaneous emission dominant regime and the stimulated emission dominant regime are examined with emission spectra and emission lifetime analyses.

*Present address: Max-Planck-Institut für Festkörperforschung, Heisenbergstrasse 1, D-7000 Stuttgart 80, Germany
†Present address: Max-Planck-Institut für Polymerforschung, Postfach 3148, D-6500 Mainz, Germany

0306–8919/92

1. Introduction

Lately, a lot of interest has been focused on the spontaneous emission properties of materials in microcavities. These structures are resonators having at least one dimension size on the order of a wavelength. In the framework of the Fermi golden rule, the effect of optical confinement in one or more dimensions is understood as a rearrangement of the usual free space density of photon states [1, 2]. The density of photon states (mode density) at some frequencies will be increased, whereas at others, it will be decreased. Furthermore, this increase or decrease will be accompanied by a spatial redistribution of mode density. Thus, if a photon emitting medium is introduced into such a cavity, its spontaneous emission rate and spatial emission intensity distribution will be altered, depending on the cavity-mode density at the emission frequency. In the last decade, much work has been done in this research field, which is called 'cavity quantum electro-dynamics (cavity QED)', particularly as a means of studying the interaction of matter with vacuum field fluctuations. To date, many experiments have demonstrated such effects, using Rydberg atoms [3–9], organic dyes [10–12], and semiconductors [13–15].

Altering the spontaneous emission, however, is also interesting from the device application point of view [16–20]. Of particular interest is the concept of a threshold-less laser proposed by Kobayashi *et al.* [16]. Recent successful demonstration of controlling spontaneous emission [12, 14, 15] and nearly threshold-less laser operation [20] using condensed materials hold technological promise for constructing ultralow power consumption semiconductor lasers. It should be noted that after the first success in the current injection vertical cavity surface emitting laser (VCSEL) [21], marked progress has been seen in constructing high performance VCSELs [22–25]. For example, submilliampere VCSELs with a very short cavity structure have been fabricated [25]. Further technological progress in these VCSEL will be naturally combined with the cavity QED approach. Changes in spontaneous emission properties could play an important role in these devices.

In this paper, we describe the spontaneous emission and laser oscillation properties of optical microcavities. In Section 2, the basic principles of the spontaneous emission alteration in microcavities are discussed within the framework of the Fermi golden rule. It is shown that two- or three-dimensionally confined microcavity structures have to be employed to induce large changes in the spontaneous emission rate. However, strong modifications of spontaneous emission pattern occur even for one-dimensional confinement structures with pairs of planar reflectors (planar microcavities). Thereafter, particular attention is paid to planar microcavities since all the experiments described were carried out using planar microcavities. Experimental studies are described in Section 3, on spontaneous emission from planar microcavities containing GaAs quantum wells or dye-embedded Lagmuir–Blodgett films. Section 4 describes the operation principle of microcavity lasers, in which controlled spontaneous emission plays an important role. A very large coupling of spontaneous emission into a cavity mode results in a laser which has no apparent threshold in the input–output curve, and this can be called the threshold-less laser. Nearly threshold-less laser operation is shown in Section 5, employing planar microcavities containing a dye solution. Prospects for microcavity devices are also discussed.

2. Alteration of spontaneous emission in microcavities

2.1. Fermi golden rule formula

First, we discuss the enhancement of the spontaneous emission rate in a closed microcavity like a wavelength-sized sphere or cube surrounded by a highly reflective material. Here, we

assume that only one resonant cavity mode overlaps the emission bandwidths of a light emitting medium because of the very small (wavelength-sized) cavity. Consider the situation in which the gain bandwidth is much smaller than the cavity mode band width. In this case, according to the Fermi golden rule, the spontaneous emission rate A in a resonant cavity is represented by [2]

$$A = \frac{2\pi}{\hbar^2 c} |\langle f|H|i\rangle|^2 \rho(k) = FA_f \tag{1}$$

with

$$F = \frac{\rho(k)}{\rho_f(k)} = \frac{2Q\pi^2}{Vk^3} \tag{2}$$

where A_f is the spontaneous emission rate in free space (hereafter, we use the words 'free space' as the meaning of 'without a cavity'), $\rho(k)$ ($\rho_f(k)$) is the mode density for a final photon state in a cavity (in free space) at transition frequency $\nu(k = 2\pi\nu/c)$, Q is the cavity quality factor, c is the velocity of light, V is the mode volume (in this case, cavity volume), H is an interaction Hamiltonian, $|i\rangle$ is the initial state without photons, and $|f\rangle$ is the final state with one photon. Then, F represents the enhancement of the spontaneous emission rate caused by the cavity. If the cavity is off-resonant, the mode density is remarkably reduced, and spontaneous emission will be suppressed. Classically, this mode density increase (or decrease) can be understood as the resonant enhancement (or anti-resonant destruction) of the emitted electro-magnetic field in the cavity. Thus, the enhanced (or suppressed) spontaneous emission is the self-reaction process of an oscillating dipole.

Alteration of spontaneous emission is induced not only in a closed (three-dimensionally confined) microcavity, but also in a two-dimensionally confined waveguide structure (optical wire) or a one-dimensionally confined planar cavity. In the following two sub-sections, we describe this issue assuming a cavity formed by *perfectly conducting mirrors*. This simplification gives us analytical solution forms for the alteration spontaneous emission rate alteration [19].

2.2. Spontaneous emission rate alteration by a planar cavity

The spontaneous emission rate given by Equation 1 can be re-expressed in another form as

$$A = \frac{2\pi}{\hbar^2 c} |M|^2 g(k) \tag{3}$$

where $g(k)$ is the effective mode density factored as

$$g(k) = \frac{1}{V} \sum_{k} P(\boldsymbol{k})\rho(\boldsymbol{k}) \tag{4}$$

Assuming a field–electric dipole interaction, $P(\boldsymbol{k})$ describes the angle dependence of the dipole matrix element $|e\boldsymbol{d} \cdot \boldsymbol{E}(\boldsymbol{k})|^2$, and $\rho(\boldsymbol{k})$ is the mode density of the field in the $\boldsymbol{k}$ direction at wavenumber k, where $e\boldsymbol{d}$ is the electric dipole moment and $\boldsymbol{E}$ is the electric field. In a microcavity, $\rho(\boldsymbol{k})$ will in general depend on the direction of the $\boldsymbol{k}$ vector. The sum proceeds over all states of wavenumber k and is normalized by the volume of the box in which the field is presumed to exist. Thus, since all the direction-dependent information is contained in $g(k)$, the matrix element M can be factored into two scalar parts; one is

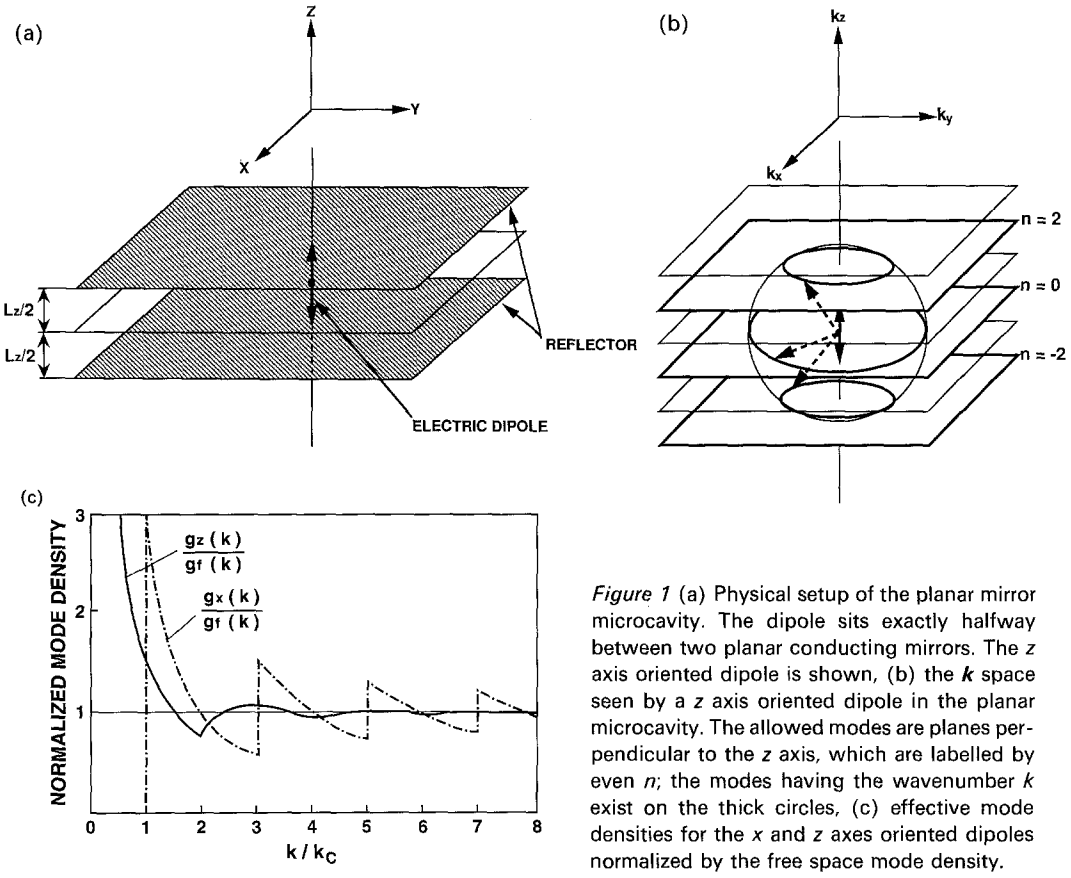

Figure 1 (a) Physical setup of the planar mirror microcavity. The dipole sits exactly halfway between two planar conducting mirrors. The z axis oriented dipole is shown, (b) the $\boldsymbol{k}$ space seen by a z axis oriented dipole in the planar microcavity. The allowed modes are planes perpendicular to the z axis, which are labelled by even n; the modes having the wavenumber k exist on the thick circles, (c) effective mode densities for the x and z axes oriented dipoles normalized by the free space mode density.

the atomic dipole matrix element for the transition from the upper to the lower level $\langle \Psi_1 | ed | \Psi_2 \rangle$ and the other is the electric field matrix element corresponding to the creation of a photon in a previously empty cavity $\langle 1 | (ck/\hbar\varepsilon)^{1/2} a^{\dagger} | 0 \rangle$, a^{+} is the photon creation operator. In this form, the quantization volume V is not included in the matrix element M because it has been moved inside $g(k)$ as shown in Equation 4. The effective mode density for a given k is found by counting the increases in the number of the allowed $\boldsymbol{k}$ vectors with unit increase in the radius of a spherical shell having radius k. Using this formula, the effective mode density seen by a dipole radiating into free space is calculated to be

$$g_f(k) = \frac{k^2}{3\pi^2}$$

We now adopt the above prescription to calculate the effective mode density seen by dipoles in a cavity consisting of two parallel plane mirrors. The physical system is depicted in Fig. 1a. The dipole is situated at the origin of a xyz coordinate system, whereas the mirrors are defined by the $z = \pm L_z/2$ planes. We must consider two possible orientations for the dipole: the vertical one (parallel to the z axis) and the horizontal one (perpendicular to the z axis). Any other orientation for the dipole can be represented as a superposition of these two cases.

Consider the structure of $\boldsymbol{k}$ space seen by the dipole between two planar mirrors. The

mirrors at $z = \pm L_z/2$ impose periodicity in the z direction on the real-space fields. Thus, in $\boldsymbol{k}$ space, allowed values of k_z exist only at a series of points centered at $k_z = 0$ and separated by a distance of π/L_z. On the other hand, the cavity is unbounded in the x–y plane; therefore, under a Fourier transform, k_x and k_y can take continuous values. Note that an allowed $\boldsymbol{k}$ at a certain value of k can exist on a circle (or circles) in an allowed x–y plane (or x–y planes) intersected by the sphere of radius k. This situation is shown in Fig. 1b. Therefore, the entire set of allowed $\boldsymbol{k}$ values is a set of planes intersecting the k_z axis at $k_z = n\pi L_z$ with integer n.

Carrying out the mode counting, the effective mode density for a z axis oriented dipole is given by

$$\begin{aligned} g_z(k) &= \frac{1}{V}\sum_{\boldsymbol{k}} P(\boldsymbol{k})\rho(\boldsymbol{k}) \\ &= \frac{k_c k}{2\pi^2}\sum_{n\,\text{even}}\left\{1 - \left(n\frac{k_c}{k}\right)^2\right\} \end{aligned} \tag{5}$$

Here, the quantization volume is taken to be $V = L^2 L_z$, and k_c is the cut off wavenumber defined as π/L_z. The last term in the second equation in brackets represents the function corresponding to $P(\boldsymbol{k})$. It should be noted that the z axis oriented dipole positioned midway between the mirrors couples only to even-order modes. This occurs because the z component of the electric field E_z varies as $\cos[n\pi(z/L_z - 1/2)]$ to match boundary conditions. The summation is taken over all integers $|n| < k/k_c$.

The effective mode density for a horizontal electric dipole is calculated in the same manner. Considering an x axis oriented dipole, the effective mode density is obtained as

$$g_x(k) = \frac{k_c k}{4\pi^2}\sum_{n\,\text{odd}}\left\{1 + \left(n\frac{k_c}{k}\right)^2\right\} \tag{6}$$

Note that this dipole couples only to modes that have a field maximum at $z = 0$ and have a form of $\sin[n\pi(z/L_z - 1/2)]$. Thus, only odd-order modes are included in the sum.

The effective mode densities $g_x(k)$ and $g_z(k)$ normalized by $g_f(k)$ are shown in Fig. 1c. The curves in this figure give the increase or decrease in the atomic transition rate when all the electric dipoles are parallel to only one axis. If the orientation of the dipoles is random, the total effective mode density is given by

$$g(k) = 2/3\, g_x(k) + 1/3\, g_z(k),$$

since $g_y(k) = g_x(k)$.

Figure 1c indicates that, with a wavelength-sized planar cavity, the increase and the decrease in the spontaneous emission rate are at most three and two respectively. It should be noted that the result shown here is equal to the standard electrodynamic field solution [19], and also to the previously reported QED calculations [26–28]. However, the simplicity of the present calculation recommends it as the preferable method for analysing microcavities of any geometry.

2.3. Spontaneous emission rate alteration by a waveguide

Here, we apply the method described in 2.2. to calculate the mode density of a two-dimensional confinement waveguide (optical wire) structure. In Fig. 2a, an optical wire and the corresponding allowed modes in $\boldsymbol{k}$ space are schematically shown. It is assumed that the active material is located in the centre of the y–z cross section. If the waveguide is made by a perfect conductor, the y and z components of all the allowed $\boldsymbol{k}$ vectors become

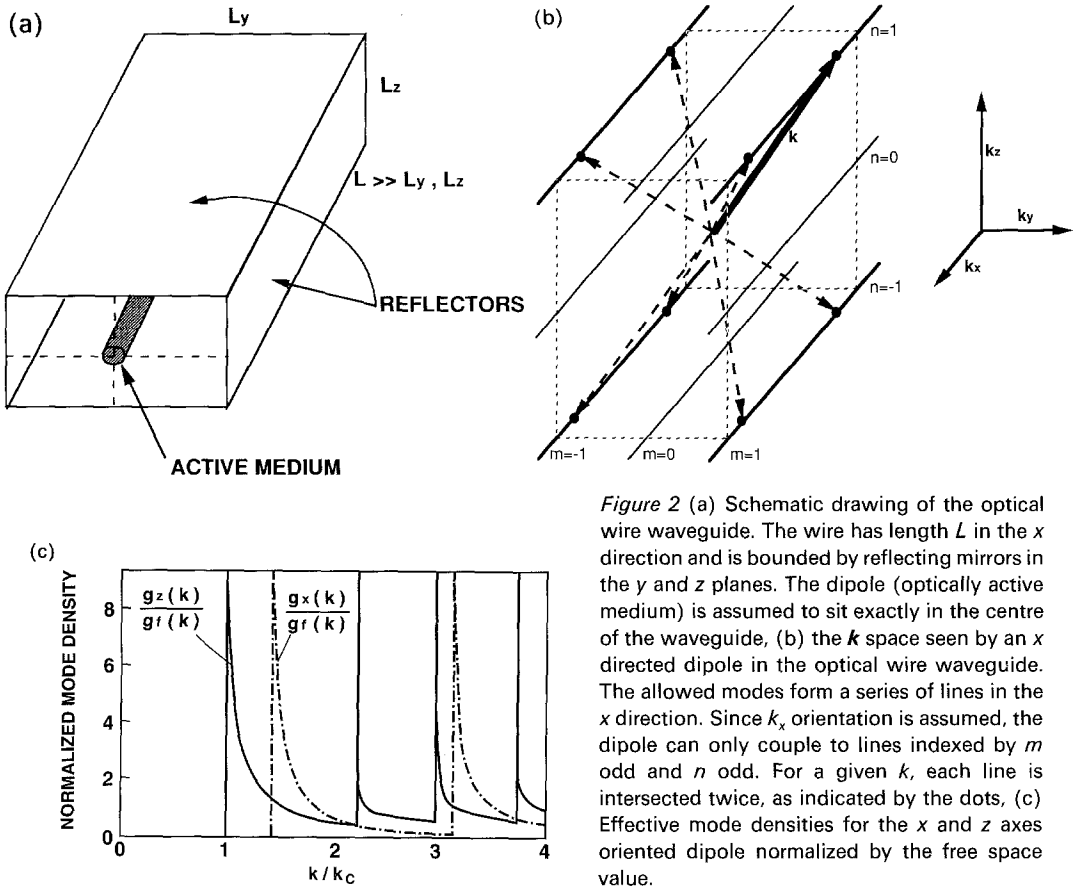

Figure 2 (a) Schematic drawing of the optical wire waveguide. The wire has length L in the x direction and is bounded by reflecting mirrors in the y and z planes. The dipole (optically active medium) is assumed to sit exactly in the centre of the waveguide, (b) the $\boldsymbol{k}$ space seen by an x directed dipole in the optical wire waveguide. The allowed modes form a series of lines in the x direction. Since k_x orientation is assumed, the dipole can only couple to lines indexed by m odd and n odd. For a given k, each line is intersected twice, as indicated by the dots, (c) Effective mode densities for the x and z axes oriented dipole normalized by the free space value.

discrete. When the length of the cavity L is much larger than the wavelength (i.e. $L \gg L_y$, L_z), the x component of $\boldsymbol{k}$ can be regarded as a continuous quantity. The allowed $\boldsymbol{k}$ space modes then form a series of parallel lines in the k_x direction separated by π/L_y in the k_y direction, and by π/L_z in the k_z direction. Depending on the orientation of the radiating dipole, only certain modes will be excited, while others will be disallowed. The mode density is obtained by counting the number of allowed modes contained on the surface of a sphere of radius $|\boldsymbol{k}|$ centred on the origin in $\boldsymbol{k}$ space. For an electric dipole parallel to z axis, the volume normalized effective mode density $g_z(k)$ is

$$g_z(k) = \frac{1}{V}\sum_{\boldsymbol{k}} P(\boldsymbol{k})\rho(\boldsymbol{k})$$

$$= \frac{1}{2\pi L_y L_z}\sum_{m\,\mathrm{odd}}\sum_{n\,\mathrm{even}} \frac{2k}{\{k^2 - [(mk_{cy})^2 + (nk_{cz})^2]\}^{1/2}} \cdot \left[1 - \left(\frac{nk_{cz}}{k}\right)^2\right] \qquad (7)$$

In the first equation, this time, the quantization volume is taken to be $V = LL_yL_z$. In the second equation, $k_{cy} = \pi/L_y$ and $k_{cz} = \pi/L_z$ are respectively the cut off wavenumbers for y and z directions, and the summation is taken over all integer m and n satisfying $k^2 \geqslant [(mk_{cy})^2 + (nk_{cz})^2]$. The allowed modes are odd m and even n because of the boundary conditions introduced by the perfect conductor, and the dipole is situated exactly in the

middle of the waveguide cross section. If the dipole is parallel to the y axis, m and n, as well as k_{cy} and k_{cz} are interchanged.

When the dipole is parallel to the x axis (parallel to the open axis of the wire), the effective mode density becomes

$$g_x(k) = \frac{1}{2\pi L_y L_z} \sum_{m\,\text{odd}} \sum_{n\,\text{odd}} \frac{2k}{\{k^2 - [(mk_{cy})^2 + (nk_{cz})^2]\}^{1/2}} \cdot \left[\frac{(mk_{cy})^2 + (nk_{cz})^2}{k^2}\right] \quad (8)$$

This is the situation depicted in Fig. 2b.

In Fig. 2c, the normalized effective mode densities $g_x(k)/g_f(k)$ and $g_z(k)/g_f(k)$ are plotted for the case $L_y = L_z$. When the orientation of the light emitting dipoles is random, the total effective mode density is given by

$$g(k) = 1/3\,[g_x(k) + g_y(k) + g_z(k)]$$

As depicted in Fig. 2c, the mode density ratio becomes infinite when $k = k_c$. For a real waveguide structure, however, the finite loss of the reflector should be taken into account. This results in a broadening of the mode peaks. Furthermore, for broad emission width materials like semiconductors, the spontaneous emission rate A is represented by

$$A = \int_0^\infty g(k)R(k)\mathrm{d}k \quad (9)$$

where $R(k)$ is essentially a factor corresponding to the optical transition matrix element, and it approximately corresponds to the spectral shape of the free space spontaneous emission. Thus, media having broad emission spectra will display smaller emission enhancement than those having narrow emission spectra, since they will sample a larger spectral region than just the peak of the effective mode density.

An estimate of the effect of an emitting medium with finite bandwidth can be obtained by considering the spectral width of GaAs, where $\Delta\lambda/\lambda_0 \sim 0.02$. Assuming $L_y = L_z = \lambda/2$ for the waveguide, the enhancement factor η is ~ 12. On the other hand, η is only 2.5 for the planar cavity of $L = \lambda/2$. This simple calculation illustrates the importance of restricted dimensionality in increasing the spontaneous emission rate. In other words, the confinement of spontaneously emitted photons into a smaller volume can induce a larger emission rate change.

A word should be said about the adaptability of the present calculations to experimental realizations of microcavities. These will be quite adequate in microwave region because it is rather easy to make an extremely low loss cavity with a superconductor. On the other hand, in optical regions, it may be necessary to use multilayer dielectric stacks for highly reflective mirrors which have a large penetration depth and a very limited reflection bandwidth, as well as rather strong incident angle dependence of the reflectivity. Thus, a quantitative comparison between the present calculations and the experiments will be difficult. However, the qualitative results we find will still be applicable to optical experiments.

Recently, a few authors have tried to calculate the spontaneous emission rate change by more realistic optical microcavity structures made by dielectric multi-layer reflectors [29–31]. Progress in these theoretical works will enable quantitative analyses of experimental results.

2.4. Spontaneous emission distribution alteration by a planar cavity

In the previous two subsections, attention has been focused on alteration of the spontaneous emission rate. Here, we discuss the change in spatial distribution of spontaneous emission

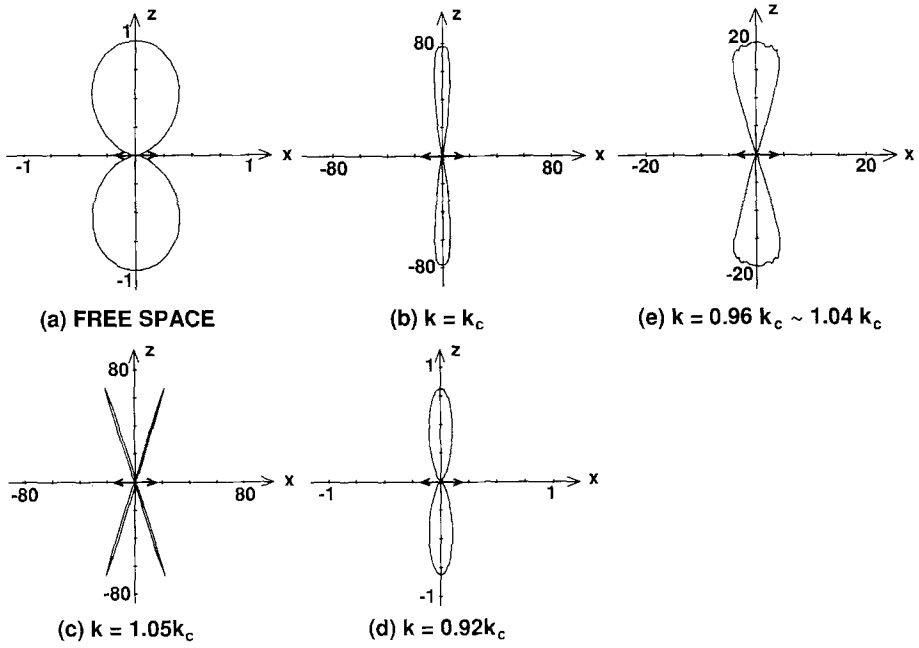

Figure 3 Emission intensity distribution patterns of dipole directed to x axis; the views from y axis. (a) free space emission, (b)–(e) emission from the dipoles located at the midway inside the $\lambda/2$ planar cavity and having different transition frequencies. It is assumed that the field is polarized in x–z plane.

intensity caused by a microcavity. Again, we focus the discussion on planar cavity structures because all the experiments performed were carried out with planar cavity structures.

For simplicity, an imaginary optical planar cavity similar to Fig. 1a is again assumed, but a finite transmission loss is introduced in the present analysis. Then, the spatial radiation pattern of the spontaneous emission is calculated using the reversible principle [10], i.e. seeing how the atomic absorption of radiation is modified by the cavity. Equivalently, this can be considered from the quantum mechanical point of view, as due to the change in zero-point fluctuation amplitude inside the cavity [15]. For example, assuming an x axis oriented electric dipole located at the midway point inside the present planar cavity and incident field polarized in x–z plane, change in the absorptivity (or the zero-point fluctuation intensity) seen from the y axis is represented by the following equation, which describes the enhancement (or suppression) of incident electromagnetic fields in a FP étalon.

$$\frac{I}{I_0} = \frac{(1 - R)(1 + R + 2(R)^{1/2} \cos(kL_z \cos\theta + \pi)) \cos^2\theta}{1 + R^2 - 2R \cos(2kL_z \cos\theta + 2\pi)} \tag{10}$$

Where I_0 is the incident field intensity and I is the field intensity seen by the dipole, R is the power reflectivity of the reflectors, and θ is the incident angle in x–z plane. Here, it is assumed that the absorbance inside the cavity is extremely small, then the absorptivity of an atom or the zero-point fluctuation intensity is factored by Equation 10. The curves depicted in Fig. 3 show this function at different dipole frequencies for a $\sim\lambda/2$ cavity assuming a reflectivity $R = 0.95$. The distance between a point on the curve and the origin corresponds to the emission intensity. The emission intensity distribution in free

space is also shown in Fig. 3a for comparison; free space emission intensity into z axis direction is normalized to be unity. Note that the same emission intensity distribution pattern is expected in a large cavity having a separation much larger than the emission wavelength. For a monochromatic dipole having a wavenumber equal to the cut-off wavenumber $k_c = \pi/L_z$, the emission intensity around the cavity axis direction is enhanced by a factor of $2(1 + R)/(1 - R) \approx 80$ as shown in Fig. 3b, and the emission is greatly suppressed in the other directions. When the dipole's wavenumber is slightly larger than k_c, as is shown in Fig. 3c, the emission cone spreads off the cavity axis. On the other hand, if the dipole's wavenumber is smaller than k_c, Fig. 3d, the emission intensity is decreased in all the directions; this is consistent with 'inhibited spontaneous emission [2]' below k_c as shown in Fig. 1c. Considering again such condensed materials as semiconductors or dyes, we must remember that the emission will be broadband rather than monochromatic. Figure 3e corresponds to this situation. A $\pm 4\%$ emission width is assumed. This result indicates that, even with a $\sim\lambda/2$ cavity, the directionality of the spontaneous emission in the cavity axis deteriorates if the laser medium has a very broad emission bandwidth. However, some directionality is still expected in comparison with a conventional 'large' cavity case corresponding to Fig. 1a. It should be noted that, even if randomly oriented dipoles are assumed instead of single axis oriented dipoles, the characteristics described do not change significantly.

3. Experiments of spontaneous emission in planar optical microcavities

3.1. GaAs quantum well microcavities

Initially, we had observed a spontaneous emission alteration of GaAs quantum wells (QWs) in a monolithic nonlinear Fabry–Perot (FP) étalon structure made by molecular beam epitaxy (MBE). The structure and the photoexcitation luminescence (PL) spectra observed from the cavity axis are shown in Fig. 4 and 5 respectively. Since the spectral shape does not change by decreasing the excitation intensity to a very low level, this strong modulation of the QWs' PL spectra is due to spontaneous emission modified by the cavity structure rather than laser oscillation. In the initial stage of VCSEL research, there were several reports misinterpreting this kind of modulated spontaneous emission as laser oscillation.

In order to see more clearly the influence of the cavity on the spontaneous emission

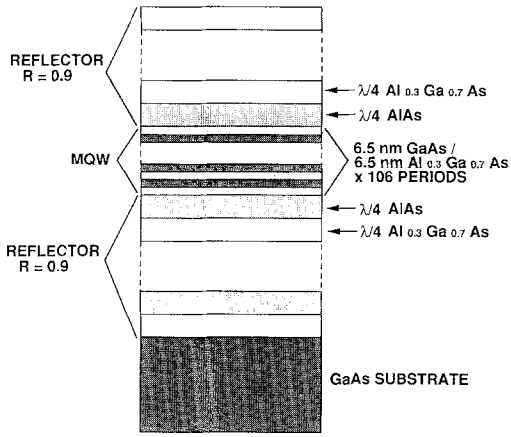

Figure 4 Schematic of an all MBE grown monolithic MQW FP étalon structure.

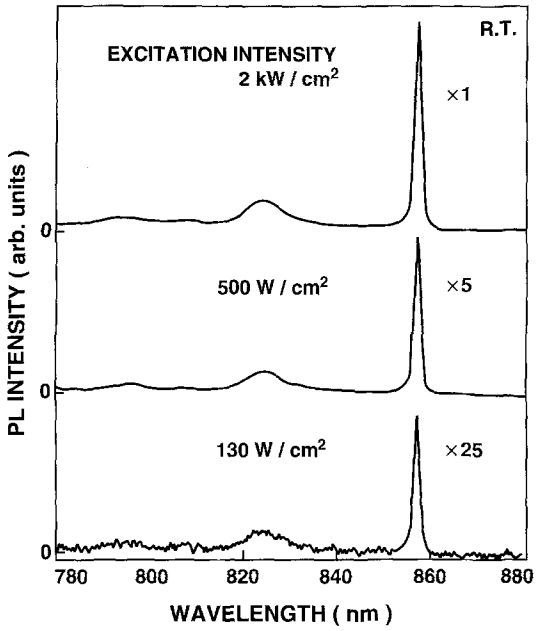

Figure 5 Room temperature PL spectra of an MQW étalon observed from the cavity axis direction under different excitation intensities.

spectrum, the FP cavity employing an external reflector shown in Fig. 6 was also constructed. In this structure, one reflector was epitaxially grown under the multiple quantum well (MQW) layer, and the surface of the MQW layer was anti-reflection coated. In Fig. 7, emission spectra are shown for different cavity lengths. By decreasing the cavity length, it is seen that the emission intensity is concentrated in a few cavity resonance modes. (The heights and widths of the resonance peaks in the multiple peak situation are limited by the system spectral resolution of ~ 0.5 nm.) At the shortest cavity length available in this structure, spontaneous emission intensity is gathered into a single resonance peak reminiscent of laser oscillation. Note that the spectrally integrated PL intensity is slightly increased in

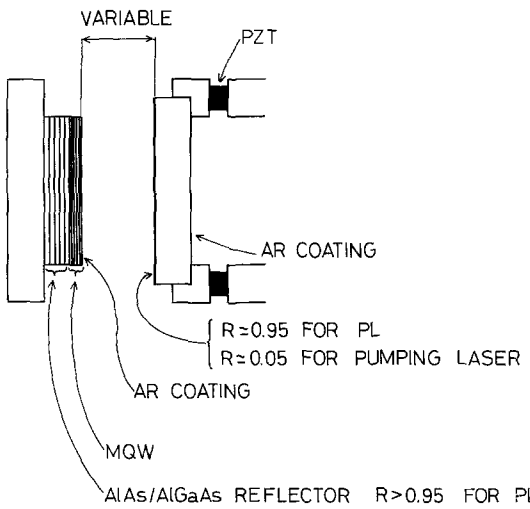

Figure 6 Schematic illustration of a GaAs MQW FP cavity employing an external reflector.

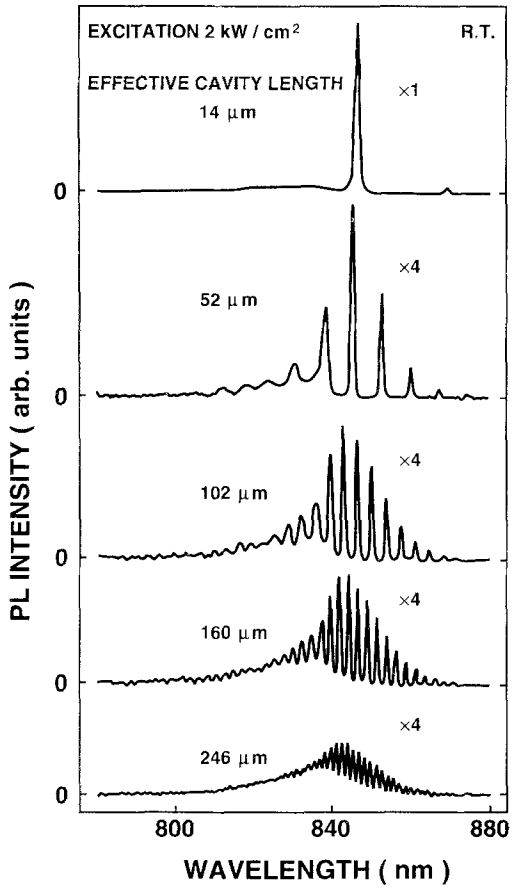

Figure 7 Room temperature PL spectra of an external mirror GaAs MQW FP cavity detected from the cavity axis direction for different cavity lengths. The envelope of the PL spectrum for the longest cavity approximate the free space PL shape.

this single mode situation compared to longer cavity cases. This seems to be the enhanced spontaneous emission described by Equation 9 within a small solid angle around the cavity axis. In an FP cavity structure, averaging over the standing wave effect, the mode density of a resonance peak is enhanced by a factor of $(1 + R)/(1 - R)$ if absorption loss is negligible. Instead of this, the resonance width is approximately given by the ratio of free spectral range and the above factor. In other words, the 'mode' condenses into a narrow resonance peak. Thus, in the situation of single resonance peak within the material's emission width, the integral of Equation 9 in the cavity axis direction can be larger than the integral without the cavity modulation of mode density; i.e. an increase in the spectrally integrated emission intensity will be observed in the cavity axis direction. Then Equation 9 is approximately represented as $P(E_0')\Delta E$ for a cavity and $P(E_0)\Delta P$ without the cavity, where $P(E)$ is the energy-dependent transition rate at photon energy E, E_0' and E_0 are the photon energies at the cavity resonance peak and free-space emission peak respectively, and ΔE and ΔP are the FP mode separation, and the full width at half maximum (FWHM) of $P(E)$ respectively. Therefore, the intensity ratio is approximately given by

$$\eta = P(E_0')\Delta E/P(E_0)\Delta P \tag{11}$$

If $E_0' = E_0$, the emission intensity is enhanced by a ratio of $\sim \Delta E/\Delta P$. Note that if $E_0' \neq E_0$,

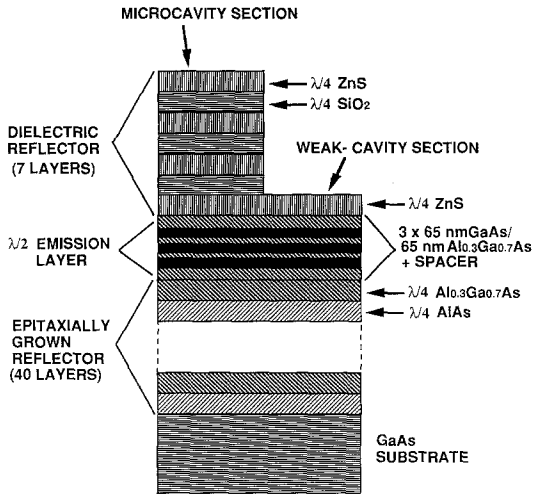

Figure 8 Schematic view of a GaAs MQW microcavity structure.

and $P(E_0)/P(E_0') > \Delta E/\Delta P$, the microcavity causes the spontaneous emission into the cavity axis direction to be suppressed instead of enhanced.

In an experiment using an atomic beam, the enhancement and suppression in the cavity axis direction have been clearly shown [8]. Note, however, that if there are multiple cavity resonance peaks within the emission width, enhancement of the spontaneous emission does not occur because the mode density increase caused by the resonance peaks is cancelled out by the mode density decrease between the resonance peaks. Thus, a quite short cavity is necessary to observe an enhancement for such condensed materials as semiconductors or organic dyes because of their very broad emission widths.

It is possible to increase the enhancement of spontaneous emission described by Equation 11 by further decreasing the cavity length because of an increase in the cavity resonance width. Therefore, we fabricated another microcavity structure shown in Fig. 8 [14]. The optical thickness of the light emitting layer is $\lambda/2$. Only the bottom reflector was made by epitaxial growth, and this was designed to yield a reflectivity of 0.98, flat over approximately 20 nm. Half of the sample wafer, hereafter called the 'microcavity section' (MCS), was covered by a seven layer ZnS/SiO_2 upper reflector having a reflectivity of ~ 0.9 for the 740–900 nm wavelength region, while showing reflectivity of less than 0.1 for wavelengths shorter than 700 nm. The other half of the wafer, hereafter called the 'weak-cavity section' (WCS), had only one ZnS upper layer as an anti-reflection (AR) coating. Note that there is a weak cavity effect in this section because of the epitaxially-grown reflector and the incomplete AR coating. For optical measurements, a small sample including both the MCS and WCS was extracted from a wafer of 40 mm in diameter. To avoid cracking the coated dielectric layers, all the measurements were carried out at room temperature.

Figure 9 shows the static PL spectra for the sample under the excitation with a He–Ne laser (the excitation spot diameter is $\sim 20\,\mu$m). The reference spectrum was obtained from a MQW sample without any reflectors. Since this comes from another wafer, its amplitude should not be compared to those from the microcavity sample. In the measurement, PL is detected along the cavity axis perpendicular to the sample surface within a solid angle of $\sim 10^{-2}\pi$. The PL spectral width for the MCS is ~ 4 nm FWHM around the lowest

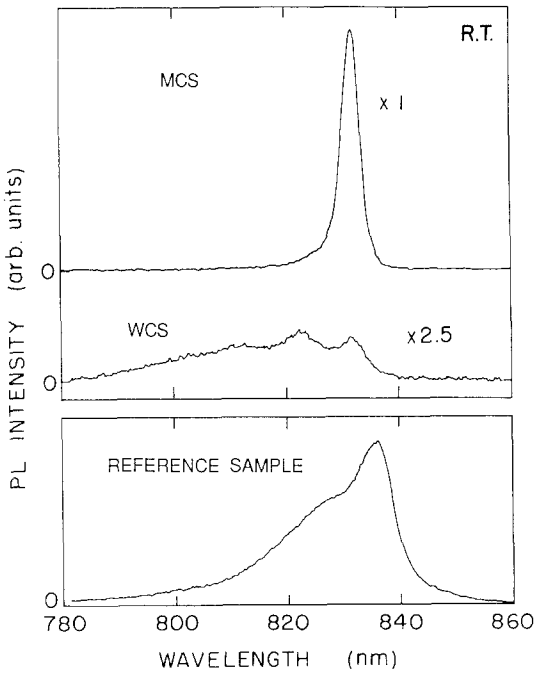

Figure 9 Room temperature PL spectra for a GaAs MQW microcavity structure. As a reference, a PL spectrum for a MQW without reflectors is also shown. Excitation He–Ne laser light intensity is 1 kW cm^{-2}, with $\sim 24\,\mu$m focal spot diameter. PL detection solid angle is $\sim 10^{-2}\pi$.

quantized electron-heavy hole transition. The PL spectrum for the WCS is modified by a residual cavity effect. The spectral shapes for both MCS and WCS do not change when the excitation intensity is varied from 1 kW cm^{-2} to 100 W cm^{-2} (the detection limit for spectra). It should be noted that the MCS and WCS, from which PL data are obtained, are less than 1 mm distant from each other on the wafer in order to assure similarity of the layer thickness and the quality of the MQW.

Figure 10 shows the spectrally integrated PL intensities of the MCS and the WCS emitted into the cavity axis direction. The PL intensity of the MCS is increased by a factor of 3.6 compared with that of the WCS. From Equation 12 we expect an enhancement factor of ~ 7 taking into account the effective cavity separation ($\sim 3\lambda$). However, considering the absorption of the MQW, the observed factor 3.6 seems to be reasonable. Note that with increasing the excitation intensity, the PL intensities for both sections show a quadratic

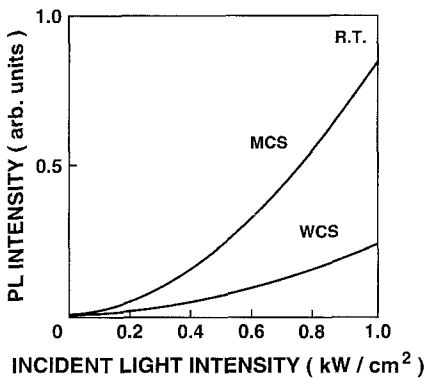

Figure 10 Spectrally integrated room temperature PL intensities for an MCS and a WCS as a function of excitation intensity.

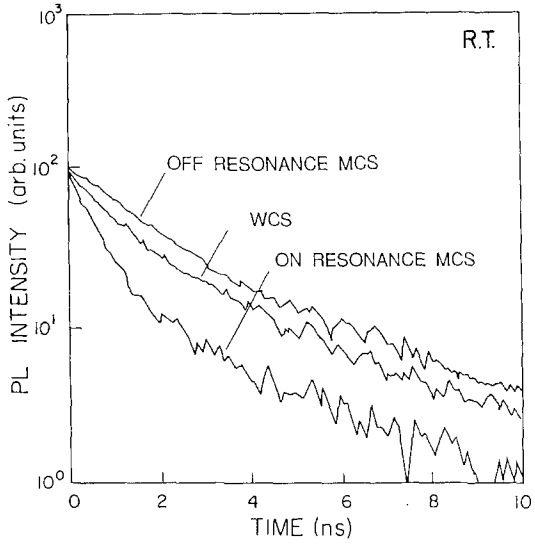

Figure 11 Room temperature PL decay traces for a GaAs MQW microcavity measured by the combination of visible diode laser's ~ 100 ps pulse excitation and single photon counting technique. In the measurement spectrally integrated PL is detected. The excited initial carrier density is $\sim 10^{18}\,cm^{-3}$. The decay times are estimated from the slope of the decay in the initial 2 ns portion of the curves.

increase. This is the feature of bimolecular radiative carrier recombination when nonradiative processes dominate the overall recombination [32]. In fact, the excited carrier density is estimated to be $\sim 10^{17}\,cm^{-3}$ at 1 kW cm^{-2} excitation intensity, taking into account the mesured nonradiative carrier lifetime of ~ 2 ns. Net stimulated emission does not occur at this carrier density. Furthermore, even if we assume a gain of $10^3\,cm^{-1}$ under intense excitation ($\gg 10^{18}\,cm^{-3}$ carrier density), the single pass gain of $\sim 4 \times 10^{-3}$ can not compensate the single pass cavity loss of 0.06 for the present rather low quality factor cavity. That means stimulated emission is negligible in the present excitation condition. Therefore, the observed emission intensity is clearly due to the enhanced spontaneous emission in the cavity axis direction.

Thus far, we have discussed changes of the PL intensity in the cavity axis direction. However, the presence of the cavity can also alter the total spontaneous emission rate as discussed in Section 2. We have examined these effects with time-resolved PL measurements. An AlGaInP visible diode laser driven by a nanosecond pulse current was used as the excitation source, which generate one hundred picosecond optical pulses of 660 nm wavelength; the decay of the emitted PL was monitored in time using the single photocounting technique [33].

From the time-resolved PL measurement, the nonradiative carrier recombination lifetime of the MQW structure has been determined to be ~ 2 ns at room temperature. This indicates that the well/barrier interfacial recombination velocity is rather large. Although a radiative recombination lifetime change cannot be observed at an initial carrier density lower than $10^{17}\,cm^{-3}$ because of the very short nonradiative lifetime, the lifetime difference between the MCS and WCS becomes measurable at higher excitation conditions. As explained previously, the contribution of stimulated emission is quite unimportant in the present structure. In Fig. 11, the decay of the spectrally integrated PL intensity is shown for $\sim 10^{18}\,cm^{-3}$ initial carrier density. The slope of the initial PL decay trace gives a decay time constant of ~ 0.6 ns for the on-resonant MCS, and ~ 1 ns for the WCS. In order to see the influence of cavity resonance condition, the off-resonant MCS, which comes from a different portion of the wafer and having a thicker light emitting layer, has also been

examined and is shown in Fig. 10; the decay time constant is almost the same as that of the WCS. The observed PL lifetime τ_T is related to the nonradiative lifetime τ_{nr}, and the radiative lifetime τ_{rad} by $1/\tau_T = 1/\tau_{nr} + 1/\tau_{rad}$. Although the estimated value of radiative lifetime τ_{rad} sensitively depends on the value of τ_{nr}, using the above relation and the measured nonradiative lifetime $\tau_{nr} \sim 2$ ns, we find radiative lifetimes around 2 ns for the WCS and off-resonant MCS, and 1 ns for the on-resonant MCS. The reduction of the radiative lifetime from 2 ns to 1 ns directly reflects the spontaneous emission rate enhancement by the microcavity. However, a clear increase in the radiative lifetime, i.e. the suppressed spontaneous emission has not been detected with any samples extracted from the present wafer. The unchanged lifetime of the present off-resonant MCS seems to be reasonable in conjunction with the calculation shown in Fig. 1c.

3.2. Dye-containing Langmuir–Blodgett film microcavities

In order to see more clearly the effect of a planar optical microcavity on the spontaneous emission lifetime change, we have also studied the microcavities having rhodamine dye embedded Langmuir–Blodgett films (LB films) [12]. Clear changes were observed in the spontaneous emission lifetime along with a modulation of the emission intensity and spectrum in the cavity axis direction.

Using an LB film offers considerable advantages by allowing the thickness to be controlled by monomolecular layer precision, while simultaneously giving reproducible high quality films. Drexhage [10] originally suggested that a spontaneous emission lifetime change should accompany modification of the radiation pattern and spectrum of dye containing Langmuir–Blodgett (LB) films deposited on metal mirrors [10]. He did not observe, however, a clear change in the spontaneous emission lifetime, because he did not fashion a cavity having high quality factor (Q factors) and he also encountered the problem of charge transfer to a metal mirror. In our structure, the entire LB film is encased between a pair of dielectric layers deposited on glass substrates.

The microcavity structure is shown in Fig. 12a. A $\lambda/6$ thick LB film containing dye is sandwiched between inert cadmium arachidate LB films. The total thickness of the LB film is adjusted by changing the number of cadmium arachidate layers. The whole LB film is gently sandwiched by a pair of dielectric mirrors, each of which consists of an 11 layer stack of $\lambda/4$ ZnS (refractive index $n = 2.3$) and $\lambda/4$ SiO_2 ($n = 1.49$) on a 5 mm thick BK7 glass substrate having $\lambda/10$ flatness precision. The highly reflective side of the mirror shows 0.985 reflectivity for a wavelength between 590 nm and 630 nm, and less than 0.2 reflectivity for the wavelengths of the excitation lasers ($\lambda < 500$ nm) for normal incidence. The other sides of the mirrors are wideband anti-reflection coated ($R < 0.01$ for $\lambda = 450$–650 nm). In the present structure, the ZnS layer contacts the LB film whose refractive index is 1.52, then standing wave nodes exist at the ZnS–LB film interface if the LB film thickness is adjusted to be a multiple of $\lambda/2$. Since the dye concentration is only 9 mol %, and the refractive indices of organic materials are usually around 1.5, we may assume the entire LB film's refractive index coincides with that of cadmium arachidate. In builing the structures, the LB film was deposited up to the designed thickness on one dielectric mirror, and the counterpart dielectric mirror was pressed softly to the LB film. For comparison with the emission properties of a film without a cavity effect, a similar structure was constructed without the $\lambda/4$ ZnS and $\lambda/4$ SiO_2 stack as shown in Fig. 12b (hereafter we call this the no-cavity structure).

Regarding the dye LB film material which is used in the experiment, several fluorescent

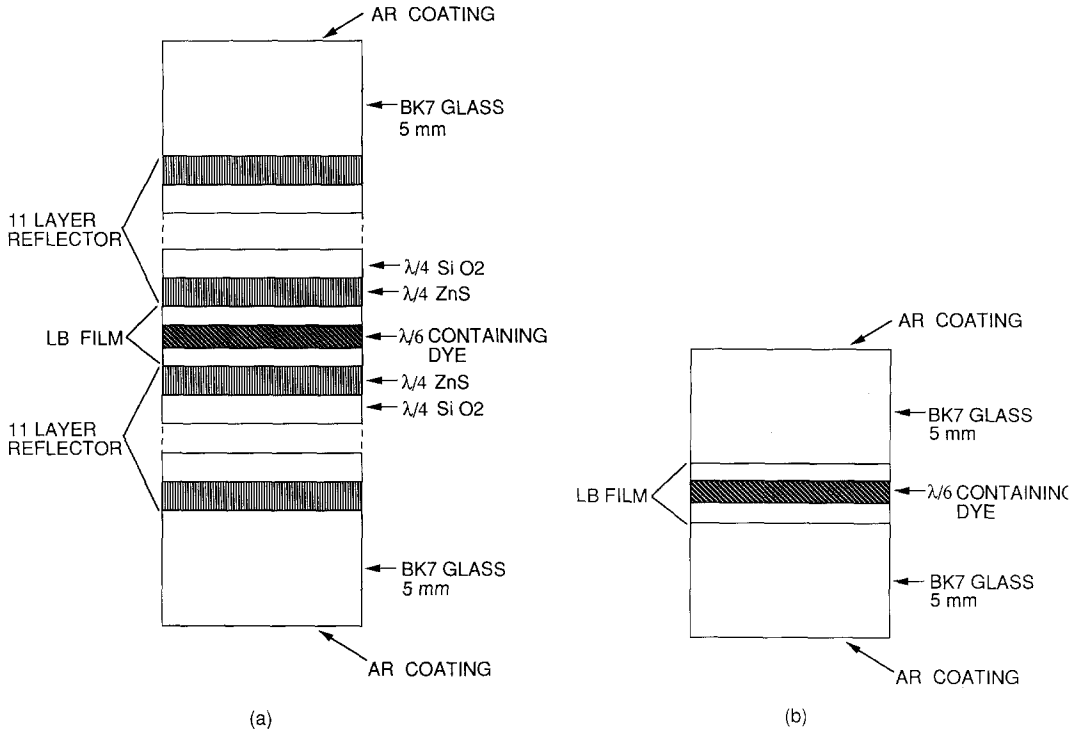

Figure 12 (a) LB film microcavity structure, (b) no-cavity structure.

dyes were screened and [9-(o-carboxyphenyl)-6-(N-ethyl-N-octadecylamino)-3H-xanthen-3-ylidene]-N-ethyl-N-octadecylammonium perchlorate (Rh) was selected for its stability and fluoresence efficiency. The thickness of the deposited Rh LB film was measured using a Taylor–Hobson 'Tally Step' instrument, and the thickness per layer was estimated to be 27.6 Å. The film structure was analysed by the conventional X-ray diffraction method. The X-ray diffraction pattern showed sharp peaks up to high order diffraction, which indicated a very good quality of deposited films. The film thickness calculated from the X-ray diffraction patterns coincided with that measured mechanically.

Photoexcitation luminescence (PL) spectra of the microcavities were measured using low power Ar ion laser (488 nm, 1 mW) excitation. It has been seen that the modulation of spontaneous emission spectra in the cavity axis direction was quite similar to that of the GaAs MQW microcavity. When the microcavity is on resonance in the cavity axis direction, the emission spectrum of the microcavity was restricted by the FP cavity resonance, and the FWHM is 4 nm. The emission intensity at the cavity resonance peak was 15 times as strong as that from the no-cavity structure at the same wavelength. This rather small value compared with the theoretical one (266) could again be due to non-negligible absorbance of the dye under the low intensity excitation. When the detection solid angle is increased to $\pi/4$ (50 mm diameter aperture), the emission FWHM of the microcavity increased to 5 nm, and the observed enhancement factor decreased to 10. This result shows that the radiation of the microcavity is rather more concentrated around the cavity axis as compared with the no-cavity structure. Although the degree of radiation concentration around

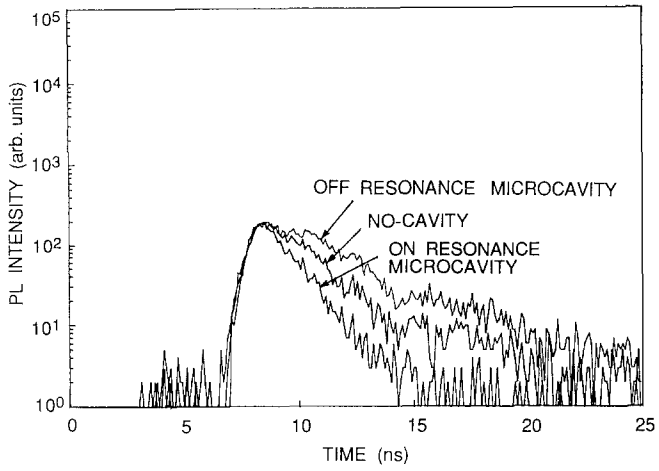

Figure 13 Spontaneous emission temporal decay curves for the on-resonant $\lambda/2$ microcavity, the off-resonant microcavity, and for the no-cavity. Spectrally integrated PL is detected in the measurement.

the cavity axis may decrease with the use of dyes which have oscillators with a variety of frequencies, the tendency will still exist. This is consistent with the calculation described in 2.4. When the cavity separation was much smaller than the on-resonance condition (i.e. off-resonance), the emission intensity was quite low, and the spectrum was not measurable.

For the PL decay time measurements, a nitrogen laser pumped Coumarine 102 dye laser (480 nm wavelength, ~ 100 ps pulse width, 60 pJ irradiation pulse energy, 30 Hz pulse repetition) was used as an excitation source. The excitation laser beam was quite loosely focused onto the LB films. The output from the microcavity was detected by the same measurement instruments described in 3.1. The measurement results are shown in Fig. 13. The three curves correspond to the on-resonant microcavity (resonance wavelength $\lambda_c = 610$ nm, decay time constant $\tau = 1$ ns), the no-cavity structure ($\tau = 1.8$ ns), and the off-resonant microcavity of 500 nm ($\lambda_c < 500$ nm, $\tau = 3.1$ ns), respectively. To compare the three decay curves, the maximum luminescence intensities are normalized to the same value in Fig. 13. We have further confirmed that all three samples show nearly the same decay times (within 1.6–1.8 ns), when the mirrors from the pair have been removed from each of the microcavities. This clearly shows that the observed emission lifetime change is induced by the presence of the microcavity.

The PL decay time of the LB film in the on-resonant microcavity is almost half of that in the no-cavity structure. This shows that the spatially integrated spontaneous emission rate was also enhanced in the on-resonant microcavity. If we assume that the no-cavity structure's PL decay time was its purely radiative spontaneous emission lifetime, the enhancement becomes nearly 2. This value seems to be consistent with the theoretical value for an ideal planar microcavity. We also observed that, when increasing the LB film thickness to over $\lambda/2$, the PL decay time approached that of the no-cavity, which is also a reasonable tendency. On the other hand, the off-resonant microcavity having the designed resonance wavelength of 500 nm showed a PL decay time longer than that of the no-cavity by a factor of 1.8. This increase again seems to be consistent with the theory. When a shorter microcavity was fabricated without C_{20} space LB films, the PL decay time was still no longer

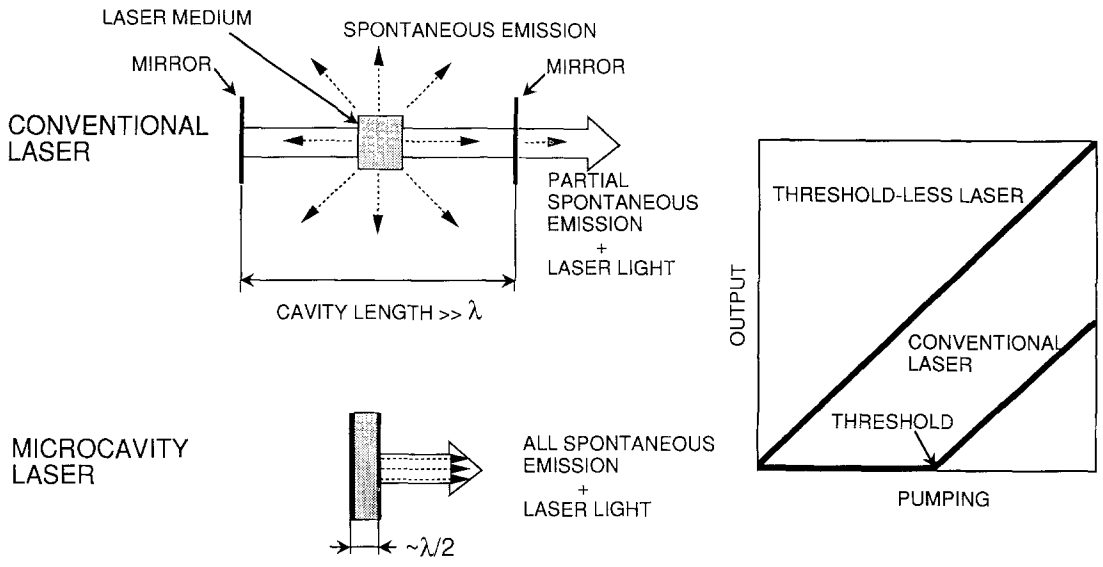

Figure 14 Schematic diagram of the operation principle of a threshold-less laser.

than 4 ns in the present experiment. This could be due to the fact that the present microcavity is not an ideal one having complete reflectors, and the dye LB film has a finite nonradiative lifetime.

It should be noted that we did not observe a measurable lifetime change when we carried out a similar experiment using several dye solutions instead of LB films. This is inconsistent with the results of DeMartini *et al.* who reported large changes in the spontaneous emission lifetime of solutions contained between dielectric mirrors [11]. In the present dye LB films, electric dipoles are located midway between the mirror pair, and could be oriented parallel to the layers, in which case the cavity effect should be stronger than in the dye solution experiment.

4. A threshold-less laser

4.1. Operation principle

In 3.1. and 3.2. we have concentrated on controlling spontaneous emission. However, as described in the introductory section, controlling spontaneous emission will induce remarkable changes in the laser oscillation properties. The most drastic effect of controlling spontaneous emission in a laser may be the threshold-less laser oscillation [16].

Figure 14 schematically represents the operation principle of a threshold-less laser. Suppose that a light-emitting material has a single narrow emission band with an extremely high quantum efficiency. In the mode point of view, the excited atoms are mostly coupled with free space modes in a conventional large sized cavity, even though there is only one cavity mode within the emission bandwidth. That is to say that most of the spontaneous emission radiates out the side of a conventional laser cavity. In that situation, the cavity mode photon number can only increase rapidly above 'threshold' due to stimulated emission. Thus, the phase transition (threshold) appears in the cavity mode output. On the other hand, in the ideal microcavity, all the emitted photons couple into the single cavity resonance mode. Therefore, increasing pumping, the emission process gradually changes

from spontaneous to stimulated emission without a phase transition (threshold) in the input–output curve.

In order to completely confine spontaneous emission into a single cavity mode, a closed microcavity structure must be ideal [16]. However, note that a very large coupling of spontaneous emission into the laser mode can be also expected with a planar microcavity because spontaneous emission concentrates around the cavity axis as discussed in 2.4.

In the next subsection, we will pay attention to changes of laser oscillation properties with the change in the ratio of spontaneous emission coupling into the laser mode.

4.2. Rate equation analysis of microcavity lasers

Although our interest has been focused on spontaneous emission in Section 2, emission rate alteration is also expected in stimulated emission. This becomes obvious with quantization of the electromagnetic field. In this procedure, the overall photon emission rate R_e for an atom in a closed cavity is expressed as

$$R_e = A(s + 1) \tag{12}$$

where s represents the number of photons in the cavity mode in the initial state.

As discussed in 2.3. the spontaneous emission rate change based on Fermi's golden rule is expected also in such broad transition linewidth systems such as organic dyes, certain solid state laser materials, and semiconductors, as long as the cavity resonance width is broader than the inverse of the radiative lifetime. However, a breakdown of the 'golden rule' often occurs in atomic systems. In this situation, coherent effects, such as Rabi oscillations [5], or 'one atom maser' operation [6] occur.

To use rate equations based on the golden rule, we must insure that the adiabatic approximation is valid. That is, no transient coherent effects occur. The phase coherence time of organic dyes and semiconductors are in the femtosecond range, while the inverse of the Rabi frequency in a cavity will be on the order of $1 \sim 10$ ps for usual optical pumping rates ($< 1\ \mathrm{MW\,cm^{-2}}$). Thus, transient coherent phenomena will not easily occur for these materials, and a rate equation approach is valid.

To begin, we may study the rate equations of a single mode microcavity laser, which is completely enclosed by the reflector. For such a device, the spontaneous emission rate is given by Equation 1. Assuming an ideal four-level laser material (the decay rates of the highest state to the upper laser state, and of the lower laser state to the lowest state are extremely fast), with no nonradiative processes and no inversion saturation, the rate equations can be written as [18]

$$\frac{dn}{dt} = p - A(s + 1)n \tag{13}$$

$$\frac{ds}{dt} = A(s + 1)n - \gamma s, \tag{14}$$

where n is the number of excited atoms (molecules) in the cavity of volume V, p represents the pumping rate, and γ is the damping rate for photons from the passive cavity. The static solution of these equations is simple but noteworthy:

$$s = \frac{p}{\gamma} \quad \text{and} \quad n = \frac{\gamma p}{A_c(p + \gamma)}.$$

We see that the light output increases linearly with increasing pumping for all pumping

rates. In other words, this device works as a threshold-less laser, as long as we focus our attention on the output versus input characteristics. As we will show, this occurs because all photons are emitted into the one single cavity mode. Note that n does not proportionally increase with an increase in pumping, and this behaviour is different from that of ordinary spontaneous emission, in which the excited state population n linearly increases with pumping increase. This threshold-less laser operation is different from that of the 'one atom maser (laser)' [6], in which a gain by single atom population inversion overcomes an extremely low cavity loss.

Although enhanced spontaneous emission ($A > A_f$) is not a necessary condition for the absence of a threshold, the consequent increase in the spontaneous emission rate has some great advantages from the device point of view. For one thing, the response speed of the device to dynamic modulation will be improved, as a result of the increased spontaneous emission rate. Another interesting feature of the threshold-less laser is that relaxation oscillations will not occur under low pumping levels. This happens because the pumping energy efficiently couples into the laser mode. Thus, the mechanism for storing energy in the laser medium, which is necessary for relaxation oscillations, is weakened. This suppressed relaxation oscillation feature is confirmed by a standard small signal analysis. The details of this analysis will be described elsewhere [32].

So far, we have considered the case of a completely closed cavity resonator. Now we would like to generalize to the case of an open resonator. We assume there is still one cavity mode, but now other modes exist which correspond to photons leaving the open cavity. We assume that the spontaneous emission into the cavity mode can still be enhanced, but the free space modes have the free space spontaneous emission rate [8]. We take the ratio of the solid angle subtended by the cavity mode to the free space modes to be β. Thus, β is proportional to the inverse of the mode volume V; from another view point, it is the light-material interaction strength because larger β results in smaller beam cross-section. If a concentric cavity [9] is assumed, the value of β simply corresponds to the solid angle in which an atom sees the cavity mirrors at the cavity centre. Also taking into account nonradiative depopulation processes, the rate equations can be represented as

$$\frac{dn}{dt} = p - (1 - \beta)A_f n - \beta A(1 + s)n - \Gamma n \tag{15}$$

$$\frac{ds}{dt} = \beta A(1 + s)n - \gamma s \tag{16}$$

Here, s is now the number of photons coupled to the cavity mode, and Γ is the nonradiative depopulation rate. Note that in a broad bandwidth material, $F = A_f/A$ depends on the cavity mode separation width as discussed in 3.1. Thus, F depends on the cavity size, as does β. Therefore, to get a large βA value, the cavity should be quite small, and to avoid the photon lifetime ($1/\gamma$) decrease, the reflectivity of cavity mirrors should be quite high. A planar microcavity with wavelength dimensions could easily provide a rather large value for β (> 0.1). Full confinement of spontaneous emission into the single cavity mode might be realized with microsphere or microcube cavity structures.

We have carried out a numerical analysis using Equations 15 and 16. Steady-state solutions for an ideal four-level laser ($\Gamma = 0$), are shown in Fig. 15 with logarithmic scales. β is the parameter in this calculation; when the spontaneous emission coupling β is quite small, clear thresholds are observed in the input–output curves. (Note that in conventional

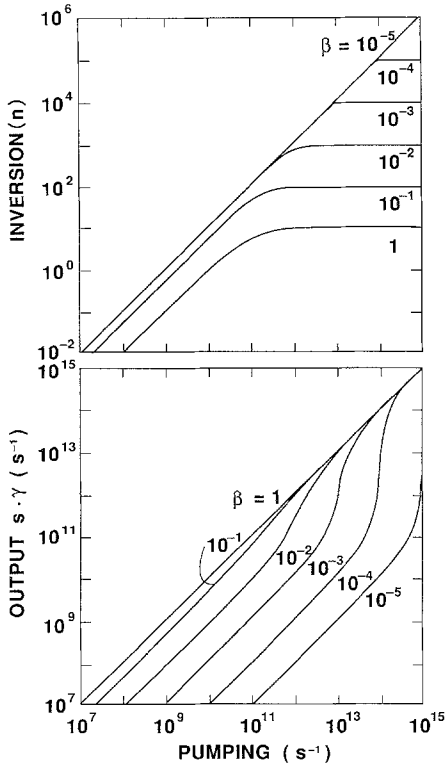

Figure 15 Calculated light output S_{out} and population inversion n versus pumping p of a microcavity four level lasers in logarithmic scales. $A = 10^9 s^{-1}$, $F = 10$, $\gamma = 10^{12} s^{-1}$ and $\Gamma = 0$.

semiconductor laser devices, β ranges from 10^{-6} to 10^{-5} per cavity mode.) It is seen, however, that the threshold becomes unclear as β increases, and it disappears in the input–output curve at $\beta = 1$. Although it may not be meaningful to distinguish spontaneous emission and stimulated emission if there is no threshold and all the photon emission processes are controlled by the cavity, for convenience, we distinguish the emission rate proportional to s in the equation as stimulated emission. If we pay attention to the behaviour of the population inversion, the difference between the spontaneous emission dominant region and the laser oscillation region is separated in the figure even for $\beta = 1$. With increasing pumping, n linearly increases within the spontaneous emission dominant region. On the other hand, in the laser oscillation region, n is clamped at the lasing threshold level. Thus, in that sense, a fuzzy threshold still exists although it does not appear in the input–output curves.

The threshold in the population inversion n $(=\gamma/\beta A)$ and also in the pumping rate (i.e. input power) decreases with increasing β. This is because of decrease in the mode volume. For a concentric cavity, in which the laser medium is located at the focal point, increasing β corresponds to an increase in the mirror size keeping the cavity length constant. This can be considered as an equivalent microcavity effect. Ujihara [33] has recently given a formula for the mode volume for a planar microcavity. Based on his formula, it is shown that the mode volume is proportional to the square of the cavity length for constant mirror reflectivity. Thus, only shortening the planar cavity's length can also decrease the threshold population inversion n because the photon dumping rate γ is only proportional to the inverse of cavity length.

It should be noted that if $\beta = 1$, the threshold pumping rate remains at $p_{th} = \gamma$ independent of A although $n_{th} = \gamma/A$ decreases with increasing A. This is reasonable since more input power is necessary to give the same n_{th} value under an increased spontaneous decay rate A.

In the operation of a microcavity laser, a very large nonradiative depopulation rate ($\Gamma \gg A$) will disturb the threshold-less laser action even at $\beta = 1$ since only stimulated emission decay can provide efficient light emission. Therefore, it is also important to use a high quantum efficiency light emitting material to achieve a threshold-less laser operation.

Although Equations 9 and 10 are valid for a four-level laser system, they are also approximately applicable to intrinsic semiconductors (with bimolecular radiative recombination). There, the spontaneous emission rate is represented by $A = B_r n$ (under the Boltzmann carrier distribution approximation), where B_r is the bimolecular carrier recombination coefficient. Furthermore, even though the inversion parameter is less than 1 (i.e. the material is absorptive at a low excitation), the condition of $\beta = 1$ can still provide threshold-less laser operation if the nonradiative decay process is negligible. When the calculation is performed using this expression for A, the features are qualitatively the same as for the case of four-level lasers.

5. Nearly threshold-less laser oscillation of planar microcavities containing a dye solution

In order to achieve threshold-less laser operation, the preferable cavity geometry is a three-dimensionally confined closed one. However, as shown in 2.4., a planar cavity may provide a rather large confinement of spontaneous emission in a single cavity resonance mode.

A 'zero-threshold laser' action was previously reported, in which a dielectric planar FP microcavity containing an organic dye solution was utilized [34]. However, the combination of a planar cavity and material having a very broad emission width such as a dye solution cannot insure a nearly full confinement of spontaneous emission into a single cavity mode. Furthermore, a rather light population inversion density in a very thin layer is necessary to achieve laser action compensating the $\sim 1\%$ single pass cavity loss. Thus, understanding the details of emission properties for the planar microcavity is a very relevant issue. We here show the results for an experimental study on the transition from spontaneous emission to laser oscillation using carefully designed planar FP microcavities containing a Rhodamine 6G solution [20]. The reasons for using Rh6G dye solution are its extremely high light emission quantum efficiency and stability. Although dye embedded LB films are excellent media for examining the spontaneous emission properties, they degrade rapidly under the rather intensive excitations necessary for laser oscillation. Semiconductor materials like MQW's in a very thin microcavity structure presently have the problem of a rather large nonradiative recombination rate, thus high quantum efficiency is not available in the spontaneous emission regime.

The microcavity structure is schematically shown in Fig. 16. It is basically quite similar to the LB film microcavity shown in Fig. 12. However, in order to precisely control the thickness of dye solution, titanium films having 200 nm thickness were partially deposited on one of the multi-layer dielectric mirrors of a F–P cavity as a spacer to introduce a dye solution (refractive index $n \sim 1.5$). Furthermore, an SiO_2 film having a thickness of an integer multiple of the half wavelength was also deposited on the remaining mirror of the F–P cavity. By changing the SiO_2 film thickness, the total distance between the mirrors was

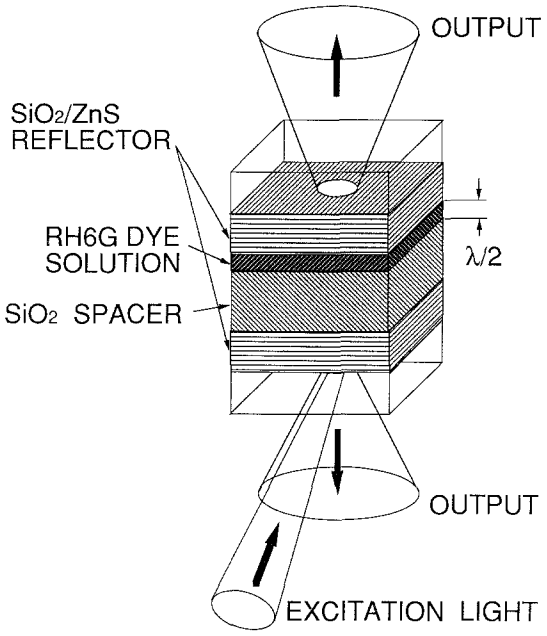

Figure 16 Planar microcavity structure containing Rh6G dye solution.

varied while keeping the dye solution thickness constant. The dielectric mirrors used consisted of 19 layers of ZnS (refractive index $n = 2.3$)/SiO_2 ($n = 1.49$)$\lambda/4$ stacks for highly reflective sides on 5 mm thick BK7 glass substrates of $\lambda/10$ flatness precision. This coating shows 0.996 reflectivity for light having a wavelength within 530–630 nm, and less than 0.2 reflectivity for wavelengths of less than 500 nm for normal incidence. The opposite side of the mirrors are wideband anti-reflection coated ($R < 0.01$ for $\lambda = 450$–650 nm). In the present geometry, standing wave anti-nodes exist midway through the dye solution layer when the thickness of the top SiO_2 film (in contact with the dye solution) is chosen as a multiple of $\lambda/2$. The space made by the Ti film was filled by capillary action with a Rhodamine 6G (Rh6G) ethanol solution of 5×10^{-3} mol dm^{-3}. For comparison with emission properties without the cavity effect, a similar structure without highly reflective dielectric layers has also been formed (hereafter we will refer to this as the no-cavity structure).

As an excitation source for laser oscillation of microcavities, a low pulse repetition rate nitrogen laser pumped Coumarine 102 dye laser ($\lambda_0 \sim 480$ nm, pulse width ~ 100 ps, pulse energy 60 nJ max., pulse repetition rate ~ 30 Hz) has been mainly used in order to avoid heating and degradation of the dye solution. An excitation laser beam 3 mm in diameter is tightly focused into the due solution portion of the microcavity by a $f = 50$ mm single lens. The theoretical limit of the excitation diameter at the focal point is approximately 3 μm. Thus, the maximum irradiation light energy density was ~ 1 J cm^{-2} (however, only 1% of the irradiation energy was absorbed). Note that this small diameter excitation geometry can avoid unintentional amplified spontaneous emission (ASE) along the dye solution layer. The output from the microcavity was collimated and focused into a 200 mm monochromator, and detected by a photomultiplier and single photon-counting electronics. The combination of a short pulse excitation scheme and single photon counting electronics enabled emission lifetime measurements. A low power Ar ion laser ($\lambda = 488$ nm, cw power 1 mW, beam

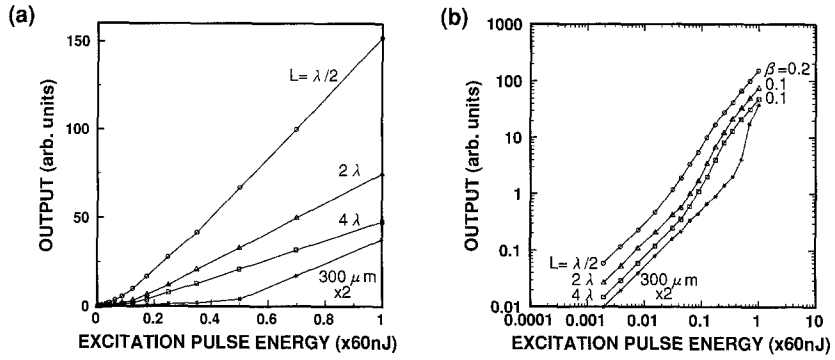

Figure 17 Light output versus excitation laser pulse energy for microcavities having three different mirror distances; (a) linear plots, (b) logarithmic plots. The cavity resonance wavelength is 560 nm for all the microcavities. For comparison, the curves for a rather long cavity are also shown. Excitation conditions: λ = 480 nm, pulse width ~100 ps, pulse repetition = 30 Hz, beam diameter ~3 mm, focused by a 50 nm focal length lens. The detection solid angle is $\sim 10^{-2}\pi$.

diameter 1 mm), and a diode laser pumped Q-switched YLF laser's second harmonic (λ = 527 nm, pulse repetition 20 kHz max., pulse energy 20 μJ max.) have also been used as excitation sources to measure the spontaneous and laser emission spectra of the microcavities. In optical measurements, the detection solid angle was fixed to $\sim 10^{-2}\pi$ around the cavity axis (10 mm diameter aperture in front of 50 mm focal length collimation lens).

Figure 17 shows the linear and logarithm plots of output versus input curves for microcavities having three different F–P cavity mirror distances ($L = \lambda/2$ means no spacer SiO_2 layer). In these microcavities, the cavity axis resonance wavelength was chosen to be 560 nm. For comparison, the curve for a rather long mirror distance cavity (200 μm thick SiO_2, e.g. ~300 μm net cavity length) was also shown. As the figure reveals, this 'long' cavity laser has a clear threshold feature. Utilizing the rate Equations 9 and 10, the coupling ratios of spontaneous emission within the measurement spectral window (~10 nm for this laser) was evaluated to be $\sim 10^{-3}$. On the other hand, lasing thresholds of microcavities are quite fuzzy, which indicates nearly threshold-laser action. This shows that the ratio of spontaneous emission coupled into the laser oscillation modes are very large in the microcavities. The coupling ratios of spontaneous emission into the lasing mode were evaluated to be ~0.2 for the $L = \lambda/2$ cavity, and ~0.1 for both the 2λ and 4λ cavities in the present experiment. It should be noted that the threshold in input, which is now defined as a transition region from the spontaneous emission dominant regime to the stimulated emission dominant regime, increased with increases in cavity length. This is, as discussed in Section 4, qualitatively consistent with the feature predicted the by Ujihara's theory [33].

Although it is not easy to clearly determine laser oscillation (stimulated emission dominant) regimes for the microcavities from the input–output curves, light emission response time measurements are useful to distinguish laser oscillation and spontaneous emission. Figure 18 shows the emission decay data for the $\lambda/2$ microcavity under three different excitation energies of 100 ps optical pulses. The decay with the lowest excitation energy corresponds to the spontaneous emission lifetime (2.2 ns). An increase in the

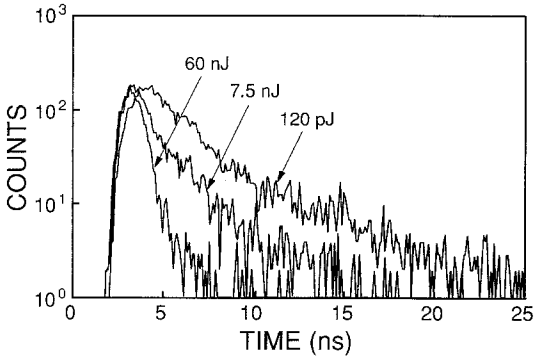

Figure 18 Emission decay curves for the $\lambda/2$ microcavity with three different excitation pulse energies. Excitation conditions are the same as those in Fig. 17.

excitation energy resulted in faster decay due to stimulated emission. The decay with the 60 nJ excitation is limited by the measurement system response (~ 300 ps).

The emission spectra of the microcavities are shown in Fig. 19. The spontaneous emission spectra and the laser emission spectra were respectively measured under excitation with weak Ar ion laser light and the second harmonic of the Q-switched YLF laser. There are no drastic changes between spontaneous and laser emission spectra, although narrowing is recognized at the foot of the peaks when stimulated emission is dominant. This is due to the fact that even spontaneous emission is restricted by the single F–P cavity resonance curve. (The intensities of laser spectra were not compared to each other because of the optical pass alignment problem.)

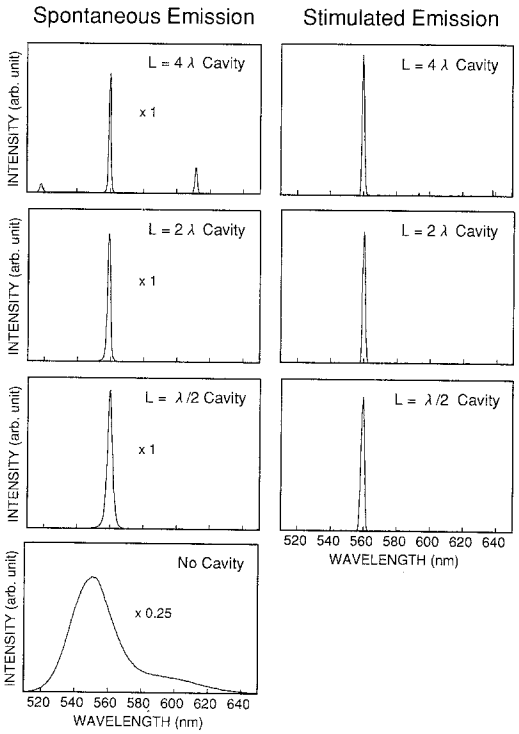

Figure 19 Spontaneous and stimulated emission spectra of the microcavities and the no-cavity structure. The detection solid anlge is $\sim 10^{-2}\pi$. $\lambda = 560$ nm, $L = \lambda/2$.

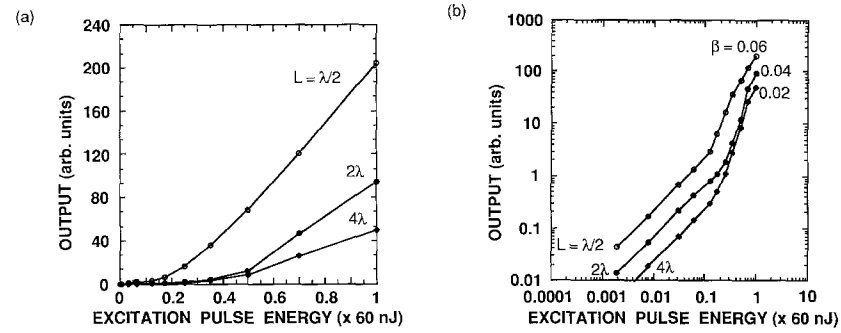

Figure 20 Light output versus excitation laser pulse energy for three microcavities; (a) linear plots when the cavity resonance wavelength is tuned to be 600 nm, (b) logarithmic plots. Excitation conditions are the same as those in Fig. 17.

When the resonance wavelength in the cavity axis direction was chosen to be 600 nm, thresholds in the input–output curves became clearer than the those at the 560 nm oscillation wavelength, as shown in Fig. 20. The evaluated coupling ratios of spontaneous emission into the lasing mode decreased to 0.06 for the $L = \lambda/2$ cavity. The higher spontaneous emission coupling efficiency at 560 nm oscillation may be attributed to the larger extraction of spontaneous emission by the cavity resonance curve as understood from the emission spectrum of Rh6G shown in Fig. 19.

We also performed a series of similar experiments for the microcavities containing Sulf-Rhodamine 640 solution. The results were quite similar to those of the Rh6G microcavities.

7. Conclusions

We have theoretically and experimentally studied spontaneous emission and laser oscillation properties of optical microcavity structures having dimensions of the emitted light wavelength. Particular attention has been paid to planar microcavity structures. We have shown that the presence of a cavity causes great modifications in the light emission spectrum and spatial emission intensity distribution, accompanied by changes in the spontaneous emission lifetime. Spontaneous emission experiments have been carried out with planar microcavities containing GaAs MQWs or organic dye embedded LB films. Regarding the laser oscillation properties, an analysis has shown that a very large coupling of spontaneous emission into a laser mode makes the lasing threshold in the input–output curve unclear, and a threshold-less laser can be achieved if all the spontaneous emission is confined in a single cavity mode. Nearly threshold-less laser operation was demonstrated using planar optical microcavities confining an organic dye solution. Differences between the spontaneous emission dominant regime and the stimulated emission dominant regime have also been observed.

Although changes in the static laser oscillation property have been discussed in the present paper, it should be noted that the microcavity laser will offer the ultrafast response (over 100 Gbps) which cannot be achieved in a conventional diode laser. One reason is due to the extremely short photon lifetime in an appropriately designed microcavity accompanied with the extremely short cavity length [32, 35]. The other reason for the response speed

increase is the cavity enhanced spontaneous emission rate [18]; two- or three-dimensionally confined microcavity structures should be fabricated for this purpose.

Another interesting subject of the microcavity optical device is the photon statistics of light output. For example, other authors have pointed out the possibility of generating number state light from a microcavity semiconductor diode laser with a very low excitation power [15]. This may be possible in the near future with further progress in VCSEL devices.

The application of cavity QED for optical devices has just started. This approach will hopefully produce novel kinds of light sources beyond conventional lasers.

Acknowledgement

The authors are grateful to K. Shimoda, H. A. Haus, Y. Yamamoto, G. Björk, E. Yablonovitch, and K. Ujihara for their discussions. The helpful comments and support of M. Sakaguchi, R. Lang, K. Asakawa, K. Onabe, H. Yamada, and K. Kosaka are also gratefully acknowleged.

References

1. E. M. PURCELL, *Phys. Rev.* **69** (1946) 681.
2. D. KLEPPNER, *ibid.* **47** (1981) 233.
3. A. G. VAIDYANATHAN, W. P. SPENCER and D. KLEPPNER, *ibid.* **47** (1981) 1592.
4. P. GOY, J. M. RAIMOND, M. GROSS and S. HAROCHE, *ibid.* **50** (1983) 1903.
5. D. MESCHEDE, H. WALTHER and G. MÜLLER, *ibid.* **54** (1985) 551.
6. G. REMPE and H. WALTHER, *ibid.* **58** (1987) 353.
7. W. JHE, A. ANDERSON, E. A. HINDS, D. MESCHEDE, L. MOI and S. HAROCHE, *ibid.* **58** (1987) 666.
8. D. J. HEINZEN, J. J. CHILDS, J. E. THOMAS and M. S. FELD, *ibid.* **58** (1987) 1320.
9. D. J. HEINZEN and M. S. FELD, *ibid.* **59** (1987) 2623.
10. K. H. DREXHAGE, in 'Progress in Optics', edited by E. Wolf (North Holland, Amsterdam, 1974), Vol. XII, p. 165.
11. F. DeMARTINI, G. INNOCENTI, G. R. JACOBOVITS and P. MATALONI, *Phys. Rev. Lett.* **59** (1987) 2995.
12. M. SUZUKI, H. YOKOYAMA, S. D. BRORSON and E. P. IPPEN, *Appl. Phys. Lett.* **58** (1991) 998.
13. E. YABLONOVITCH, T. J. GMITTER and R. BHAT, *Phys. Rev. Lett.* **61** (1986) 2546.
14. H. YOKOYAMA, K. NISHI, T. ANAN and H. YAMADA, 'Tech. Digest of Topical Meeting on Quantum Wells for Optics and Optoelectronics', Salt Lake City, March 1989, paper MD4, H. YOKOYAMA, K. NISHI, T. ANAN, H. YAMADA, S. D. BRORSON and E. P. IPPEN, *Appl. Phys. Lett.* **57** (1990) 2814.
15. Y. YAMAMOTO, S. MACHIDA, K. IGETA and Y. HORIKOSHI, 'Tech. Digest of 6th Rochester Conference on Coherence and Quantum Optics', Rochester, June 1989.
16. T. KOBAYASHI, T. SEGAWA, A. MORIMOTO and T. SUETA, 'Tech. Digest of 43th Fall Meeting of Japanese Applied Physics Society', paper 29a-B-6 (Sep. 1982); T. KOBAYASHI, A. MORIMOTO and T. SUETA, 'Tech. Digest of 46th Fall Meeting of Japanese Applied Physics Society', paper 4a-N-1 (Oct. 1985) (both in Japanese).
17. E. YABLONOVITCH, *Phys. Rev. Lett.* **58** (1987) 2059.
18. H. YOKOYAMA and S. D. BRORSON, *J. Appl. Phys.* **66** (1989) 4801.
19. S. D. BRORSON, H. YOKOYAMA and E. P. IPPEN, *IEEE J. Quantum Electron.* **26** (1990) 1492.
20. H. YOKOYAMA, M. SUZUKI and Y. NAMBU, *Appl. Phys. Lett.* **58** (1991) 2598.
21. H. SODA, K. IGA, C. KITAHARA and Y. SUEMATSU, *Jpn. J. Appl. Phys.* **18** (1979) 2329.
22. F. KOYAMA, S. KINOSHITA and K. IGA, *Trans. IECE Jpn.*, **E71** (1988) 1089.
23. J. L. JEWELL, S. L. McCALL, Y. H. LEE, A. SCHERE, A. C. GOSSARD and J. H. ENGLISH, *Appl. Phys. Lett.* **54** (1989) 1400.
24. A. SCHERE, J. L. JEWELL, Y. H. LEE, J. P. HABRISON and L. T. FLOREZ, *ibid.* **55** (1989) 2724.
25. R. S. GEELS and L. A. COLDREN, *ibid.* **57** (1990) 1605.
26. P. W. MILONNI and P. L. KNIGHT, *Opt. Commun.* **9** (1973) 119.
27. P. STEHLE, *Phys. Rev. A* **2** (1970) 102.
28. M. R. PHILOPOTT, *Chemi. Phys. Lett.* **19** (1973) 435.

29. X. P. FENG, *Optics Commun.* **83** (1991) 162.
30. G. BJÖRK, S. MACHIDA, Y. YAMAMOTO and K. IGETA, *Phys. Rev. A.* **44** (1991) 669.
31. T. BABA, T. HAMANO, F. KOYAMA and K. IGA, *IEEE J. Quantum Electron.* **27** (1991) 1347.
32. Y. NAMBU and H. YOKOYAMA, unpublished.
33. K. UJIHARA, *Jpn. J. Appl. Phys.* **30** (1991) L901.
34. F. DeMARTINI and J. R. JACOBOVITZ, *Phys. Rev. Lett.* **60** (1988) 1711.
35. Y. NAMBU and H YOKOYAMA, 'Tech. Digest of 1991 Quantum Electronics and Laser Science Conference', Baltimore, May 1991, paper JThB1.